

DESY-02-082

4. June 2002

Measurement of diffractive production of $D^{*\pm}(2010)$ mesons in deep inelastic scattering at HERA

ZEUS Collaboration

Abstract

Diffractive production of $D^{*\pm}(2010)$ mesons in deep inelastic scattering has been measured with the ZEUS detector at HERA using an integrated luminosity of 44.3 pb^{-1} . Diffractive charm production is identified by the presence of a large rapidity gap in the final state of events in which a $D^{*\pm}(2010)$ meson is reconstructed in the decay channel $D^{*+} \rightarrow (D^0 \rightarrow K^-\pi^+)\pi_s^+$ (+ charge conjugate). Differential cross sections when compared with theoretical predictions indicate the importance of gluons in such diffractive interactions.

The ZEUS Collaboration

S. Chekanov, D. Krakauer, S. Magill, B. Musgrave, J. Repond, R. Yoshida
Argonne National Laboratory, Argonne, Illinois 60439-4815ⁿ

M.C.K. Mattingly
Andrews University, Berrien Springs, Michigan 49104-0380

P. Antonioli, G. Bari, M. Basile, L. Bellagamba, D. Boscherini, A. Bruni, G. Bruni,
G. Cara Romeo, L. Cifarelli, F. Cindolo, A. Contin, M. Corradi, S. De Pasquale, P. Giusti,
G. Iacobucci, A. Margotti, R. Nania, F. Palmonari, A. Pesci, G. Sartorelli, A. Zichichi
University and INFN Bologna, Bologna, Italy^e

G. Aghuzumtsyan, D. Bartsch, I. Brock, J. Crittenden¹, S. Goers, H. Hartmann, E. Hilger,
P. Irrgang, H.-P. Jakob, A. Kappes, U.F. Katz², R. Kerger³, O. Kind, E. Paul, J. Rautenberg⁴,
R. Renner, H. Schnurbusch, A. Stifutkin, J. Tandler, K.C. Voss, A. Weber
Physikalisches Institut der Universität Bonn, Bonn, Germany^b

D.S. Bailey⁵, N.H. Brook⁵, J.E. Cole, B. Foster, G.P. Heath, H.F. Heath, S. Robins,
E. Rodrigues⁶, J. Scott, R.J. Tapper, M. Wing
H.H. Wills Physics Laboratory, University of Bristol, Bristol, United Kingdom^m

M. Capua, A. Mastroberardino, M. Schioppa, G. Susinno
Calabria University, Physics Department and INFN, Cosenza, Italy^e

J.Y. Kim, Y.K. Kim, J.H. Lee, I.T. Lim, M.Y. Pac⁷
Chonnam National University, Kwangju, Korea^g

A. Caldwell, M. Helbich, X. Liu, B. Mellado, S. Paganis, W.B. Schmidke, F. Sciulli
Nevis Laboratories, Columbia University, Irvington on Hudson, New York 10027^o

J. Chwastowski, A. Eskreys, J. Figiel, K. Olkiewicz, K. Piotrkowski⁸, M.B. Przybycień⁹,
P. Stopa, L. Zawiejski
Institute of Nuclear Physics, Cracow, Polandⁱ

L. Adamczyk, B. Bednarek, I. Grabowska-Bold, K. Jeleń, D. Kisielewska, A.M. Kowal,
M. Kowal, T. Kowalski, B. Mindur, M. Przybycień, E. Rulikowska-Zarębska, L. Suszycki,
D. Szuba, J. Szuba¹⁰
*Faculty of Physics and Nuclear Techniques, University of Mining and Metallurgy, Cracow,
Poland^p*

A. Kotański¹¹, W. Słomiński¹²
Department of Physics, Jagellonian University, Cracow, Poland

L.A.T. Bauerdick¹³, U. Behrens, K. Borrás, V. Chiochia, D. Dannheim, M. Derrick¹⁴, G. Drews, J. Fourletova, A. Fox-Murphy, U. Fricke, A. Geiser, F. Goebel¹⁵, P. Göttlicher¹⁶, O. Gutsche, T. Haas, W. Hain, G.F. Hartner, S. Hillert, U. Kötz, H. Kowalski¹⁷, H. Labes, D. Lelas, B. Löhr, R. Mankel, M. Martínez¹³, M. Moritz, D. Notz, I.-A. Pellmann, M.C. Petrucci, A. Polini, A. Raval, U. Schneekloth, F. Selonke¹⁸, B. Surrow¹⁹, H. Wesołek, R. Wichmann²⁰, G. Wolf, C. Youngman, W. Zeuner

Deutsches Elektronen-Synchrotron DESY, Hamburg, Germany

A. Lopez-Duran Viani²¹, A. Meyer, S. Schlenstedt

DESY Zeuthen, Zeuthen, Germany

G. Barbagli, E. Gallo, C. Genta, P. G. Pelfer

University and INFN, Florence, Italy^e

A. Bamberger, A. Benen, N. Coppola, H. Raach

Fakultät für Physik der Universität Freiburg i.Br., Freiburg i.Br., Germany^b

M. Bell, P.J. Bussey, A.T. Doyle, C. Glasman, S. Hanlon, S.W. Lee, A. Lupi, G.J. McCance, D.H. Saxon, I.O. Skillicorn

Department of Physics and Astronomy, University of Glasgow, Glasgow, United Kingdom^m

I. Gialas

Department of Engineering in Management and Finance, Univ. of Aegean, Greece

B. Bodmann, T. Carli, U. Holm, K. Klimek, N. Krumnack, E. Lohrmann, M. Milite, H. Salehi, S. Stonjek²², K. Wick, A. Ziegler, Ar. Ziegler

Hamburg University, Institute of Exp. Physics, Hamburg, Germany^b

C. Collins-Tooth, C. Foudas, R. Gonçalo⁶, K.R. Long, F. Metlica, D.B. Miller, A.D. Tap-
per, R. Walker

Imperial College London, High Energy Nuclear Physics Group, London, United Kingdom^m

P. Cloth, D. Filges

Forschungszentrum Jülich, Institut für Kernphysik, Jülich, Germany

M. Kuze, K. Nagano, K. Tokushuku²³, S. Yamada, Y. Yamazaki

Institute of Particle and Nuclear Studies, KEK, Tsukuba, Japan^f

A.N. Barakbaev, E.G. Boos, N.S. Pokrovskiy, B.O. Zhautykov

Institute of Physics and Technology of Ministry of Education and Science of Kazakhstan, Almaty, Kazakhstan

H. Lim, D. Son

Kyungpook National University, Taegu, Korea^g

F. Barreiro, O. González, L. Labarga, J. del Peso, I. Redondo²⁴, J. Terrón, M. Vázquez
Departamento de Física Teórica, Universidad Autónoma Madrid, Madrid, Spain^l

M. Barbi, A. Bertolin, F. Corriveau, A. Ochs, S. Padhi, D.G. Stairs, M. St-Laurent
Department of Physics, McGill University, Montréal, Québec, Canada H3A 2T8^a

T. Tsurugai
Meiji Gakuin University, Faculty of General Education, Yokohama, Japan

A. Antonov, V. Bashkirov²⁵, P. Danilov, B.A. Dolgoshein, D. Gladkov, V. Sosnovtsev,
 S. Suchkov
Moscow Engineering Physics Institute, Moscow, Russia^j

R.K. Dementiev, P.F. Ermolov, Yu.A. Golubkov, I.I. Katkov, L.A. Khein, I.A. Korzhavina,
 V.A. Kuzmin, B.B. Levchenko, O.Yu. Lukina, A.S. Proskuryakov, L.M. Shcheglova,
 N.N. Vlasov, S.A. Zotkin
Moscow State University, Institute of Nuclear Physics, Moscow, Russia^k

C. Bokel, J. Engelen, S. Grijpink, E. Koffeman, P. Kooijman, E. Maddox, A. Pellegrino,
 S. Schagen, E. Tassi, H. Tiecke, N. Tuning, J.J. Velthuis, L. Wiggers, E. de Wolf
NIKHEF and University of Amsterdam, Amsterdam, Netherlands^h

N. Brümmner, B. Bylsma, L.S. Durkin, J. Gilmore, C.M. Ginsburg, C.L. Kim, T.Y. Ling
*Physics Department, Ohio State University, Columbus, Ohio 43210*ⁿ

S. Boogert, A.M. Cooper-Sarkar, R.C.E. Devenish, J. Ferrando, G. Grzelak, T. Matsushita,
 M. Rigby, O. Ruske²⁶, M.R. Sutton, R. Walczak
Department of Physics, University of Oxford, Oxford United Kingdom^m

R. Brugnera, R. Carlin, F. Dal Corso, S. Dusini, A. Garfagnini, S. Limentani, A. Longhin,
 A. Parenti, M. Posocco, L. Stanco, M. Turcato
Dipartimento di Fisica dell'Università and INFN, Padova, Italy^e

E.A. Heaphy, B.Y. Oh, P.R.B. Saull²⁷, J.J. Whitmore²⁸
*Department of Physics, Pennsylvania State University, University Park, Pennsylvania
 16802*^o

Y. Iga
Polytechnic University, Sagamihara, Japan^f

G. D'Agostini, G. Marini, A. Nigro
Dipartimento di Fisica, Università 'La Sapienza' and INFN, Rome, Italy^e

C. Cormack, J.C. Hart, N.A. McCubbin
Rutherford Appleton Laboratory, Chilton, Didcot, Oxon, United Kingdom^m

C. Heusch

University of California, Santa Cruz, California 95064 ⁿ

I.H. Park

Seoul National University, Seoul, Korea

N. Pavel

Fachbereich Physik der Universität-Gesamthochschule Siegen, Germany

H. Abramowicz, S. Dagan, A. Gabareen, S. Kananov, A. Kreisel, A. Levy

Raymond and Beverly Sackler Faculty of Exact Sciences, School of Physics, Tel-Aviv University, Tel-Aviv, Israel ^d

T. Abe, T. Fusayasu, T. Kohno, K. Umemori, T. Yamashita

Department of Physics, University of Tokyo, Tokyo, Japan ^f

R. Hamatsu, T. Hirose¹⁸, M. Inuzuka, S. Kitamura²⁹, K. Matsuzawa, T. Nishimura

Tokyo Metropolitan University, Department of Physics, Tokyo, Japan ^f

M. Arneodo³⁰, N. Cartiglia, R. Cirio, M. Costa, M.I. Ferrero, S. Maselli, V. Monaco, C. Peroni, M. Ruspá, R. Sacchi, A. Solano, A. Staiano

Università di Torino, Dipartimento di Fisica Sperimentale and INFN, Torino, Italy ^e

R. Galea, T. Koop, G.M. Levman, J.F. Martin, A. Mirea, A. Sabetfakhri

Department of Physics, University of Toronto, Toronto, Ontario, Canada M5S 1A7 ^a

J.M. Butterworth, C. Gwenlan, R. Hall-Wilton, T.W. Jones, J.B. Lane, M.S. Lightwood, J.H. Loizides³¹, B.J. West

Physics and Astronomy Department, University College London, London, United Kingdom ^m

J. Ciborowski³², R. Ciesielski³³, R.J. Nowak, J.M. Pawlak, B. Smalska³⁴, J. Sztuk³⁵, T. Tymieniecka³⁶, A. Ukleja³⁶, J. Ukleja, J.A. Zakrzewski, A.F. Żarnecki

Warsaw University, Institute of Experimental Physics, Warsaw, Poland ^q

M. Adamus, P. Plucinski

Institute for Nuclear Studies, Warsaw, Poland ^q

Y. Eisenberg, L.K. Gladilin³⁷, D. Hochman, U. Karshon

Department of Particle Physics, Weizmann Institute, Rehovot, Israel ^c

D. Kçira, S. Lammers, L. Li, D.D. Reeder, A.A. Savin, W.H. Smith

Department of Physics, University of Wisconsin, Madison, Wisconsin 53706 ⁿ

A. Deshpande, S. Dhawan, V.W. Hughes, P.B. Straub

Department of Physics, Yale University, New Haven, Connecticut 06520-8121 ⁿ

S. Bhadra, C.D. Catterall, S. Fourletov, S. Menary, M. Soares, J. Standage

Department of Physics, York University, Ontario, Canada M3J 1P3 ^a

- ¹ now at Cornell University, Ithaca/NY, USA
- ² on leave of absence at University of Erlangen-Nürnberg, Germany
- ³ now at Ministère de la Culture, de L'Enseignement Supérieur et de la Recherche, Luxembourg
- ⁴ supported by the GIF, contract I-523-13.7/97
- ⁵ PPARC Advanced fellow
- ⁶ supported by the Portuguese Foundation for Science and Technology (FCT)
- ⁷ now at Dongshin University, Naju, Korea
- ⁸ now at Université Catholique de Louvain, Louvain-la-Neuve/Belgium
- ⁹ now at Northwestern Univ., Evanston/IL, USA
- ¹⁰ partly supported by the Israel Science Foundation and the Israel Ministry of Science
- ¹¹ supported by the Polish State Committee for Scientific Research, grant no. 2 P03B 09322
- ¹² member of Dept. of Computer Science, supported by the Polish State Committee for Sci. Res., grant no. 2 P03B 06116
- ¹³ now at Fermilab, Batavia/IL, USA
- ¹⁴ on leave from Argonne National Laboratory, USA
- ¹⁵ now at Max-Planck-Institut für Physik, München/Germany
- ¹⁶ now at DESY group FEB
- ¹⁷ on leave of absence at Columbia Univ., Nevis Labs., N.Y./USA
- ¹⁸ retired
- ¹⁹ now at Brookhaven National Lab., Upton/NY, USA
- ²⁰ now at Mobilcom AG, Rendsburg-Büdelndorf, Germany
- ²¹ now at Deutsche Börse Systems AG, Frankfurt/Main, Germany
- ²² now at Univ. of Oxford, Oxford/UK
- ²³ also at University of Tokyo
- ²⁴ now at LPNHE Ecole Polytechnique, Paris, France
- ²⁵ now at Loma Linda University, Loma Linda, CA, USA
- ²⁶ now at IBM Global Services, Frankfurt/Main, Germany
- ²⁷ now at National Research Council, Ottawa/Canada
- ²⁸ on leave of absence at The National Science Foundation, Arlington, VA/USA
- ²⁹ present address: Tokyo Metropolitan University of Health Sciences, Tokyo 116-8551, Japan
- ³⁰ also at Università del Piemonte Orientale, Novara, Italy
- ³¹ supported by Argonne National Laboratory, USA
- ³² also at Łódź University, Poland
- ³³ supported by the Polish State Committee for Scientific Research, grant no. 2 P03B 07222
- ³⁴ supported by the Polish State Committee for Scientific Research, grant no. 2 P03B

00219

³⁵ Łódź University, Poland

³⁶ sup. by Pol. State Com. for Scien. Res., 5 P03B 09820 and by Germ. Fed. Min. for Edu. and Research (BMBF), POL 01/043

³⁷ on leave from MSU, partly supported by University of Wisconsin via the U.S.-Israel BSF

- ^a supported by the Natural Sciences and Engineering Research Council of Canada (NSERC)
- ^b supported by the German Federal Ministry for Education and Research (BMBF), under contract numbers HZ1GUA 2, HZ1GUB 0, HZ1PDA 5, HZ1VFA 5
- ^c supported by the MINERVA Gesellschaft für Forschung GmbH, the Israel Science Foundation, the U.S.-Israel Binational Science Foundation, the Israel Ministry of Science and the Benozvio Center for High Energy Physics
- ^d supported by the German-Israeli Foundation, the Israel Science Foundation, and by the Israel Ministry of Science
- ^e supported by the Italian National Institute for Nuclear Physics (INFN)
- ^f supported by the Japanese Ministry of Education, Science and Culture (the Monbusho) and its grants for Scientific Research
- ^g supported by the Korean Ministry of Education and Korea Science and Engineering Foundation
- ^h supported by the Netherlands Foundation for Research on Matter (FOM)
- ⁱ supported by the Polish State Committee for Scientific Research, grant no. 620/E-77/SPUB-M/DESY/P-03/DZ 247/2000-2002
- ^j partially supported by the German Federal Ministry for Education and Research (BMBF)
- ^k supported by the Fund for Fundamental Research of Russian Ministry for Science and Education and by the German Federal Ministry for Education and Research (BMBF)
- ^l supported by the Spanish Ministry of Education and Science through funds provided by CICYT
- ^m supported by the Particle Physics and Astronomy Research Council, UK
- ⁿ supported by the US Department of Energy
- ^o supported by the US National Science Foundation
- ^p supported by the Polish State Committee for Scientific Research, grant no. 112/E-356/SPUB-M/DESY/P-03/DZ 301/2000-2002, 2 P03B 13922
- ^q supported by the Polish State Committee for Scientific Research, grant no. 115/E-343/SPUB-M/DESY/P-03/DZ 121/2001-2002, 2 P03B 07022

1 Introduction

Diffractive interactions in neutral current deep inelastic scattering (DIS) have been studied extensively at HERA [1–7]. Both inclusive and diffractive DIS cross sections rise more rapidly with energy than is the case for soft hadronic interactions [8], indicating the presence of a hard process to which perturbative Quantum Chromodynamics (pQCD) is applicable. Charm production is a key process for investigating the dynamics of diffractive DIS [9–14], since the charm-quark mass provides a hard scale and charm production is known to be sensitive to gluon-exchange processes in DIS [15, 16].

Two contrasting approaches to describe diffractive DIS are considered in this paper:

1. Resolved-Pomeron models:

these are Regge-inspired, with an exchanged Pomeron having a partonic structure [17]. The evolution of the parton distributions of the Pomeron with Q^2 is described by the DGLAP equations [18]. Diffractive HERA data [6, 19] indicate a large gluonic component. In these models, charm is produced via boson-gluon fusion (BGF);

2. Two-gluon-exchange models:

these are based on decomposing the wave-function of the virtual photon in the proton rest frame into partonic Fock states — particularly $q\bar{q}$ and $q\bar{q}g$ [20]. These states then interact with the proton via colour-singlet exchange, the simplest form of which is the exchange of two gluons [21]. If the $q\bar{q}$ state dominates, charm production will be suppressed [22]. However, if the $q\bar{q}g$ state is dominant, similar production rates to those predicted by the resolved Pomeron model are expected [11, 13, 23]. The $q\bar{q}$ and $q\bar{q}g$ configurations populate different regions of phase space.

The “soft colour interaction” [24] and “semi-classical” [9] models give very similar predictions for charm production to the two models described above and therefore are not considered separately.

This paper describes the measurement of differential cross sections for $D^{*\pm}$ production in diffractive DIS and the ratio with inclusive DIS $D^{*\pm}$ production. The results are compared to resolved-Pomeron and two-gluon-exchange models. Similar results, including comparisons to the soft colour interaction, semi-classical and other models, have recently been published by the H1 Collaboration [25].

2 Description of the experiment

The integrated luminosity of $44.3 \pm 0.7 \text{ pb}^{-1}$ used for this measurement was collected at the ep collider HERA with the ZEUS detector during 1995 - 1997, when HERA collided

27.5 GeV positrons with 820 GeV protons, giving a centre-of-mass energy of 300 GeV.

A detailed description of the ZEUS detector can be found elsewhere [26]. A brief outline of the components that are most relevant for this analysis is given below. Charged particles are tracked in the central tracking detector (CTD) [27], which operates in a magnetic field of 1.43 T provided by a thin superconducting coil. The CTD consists of 72 cylindrical drift chamber layers, organized in 9 superlayers covering the polar-angle¹ region $15^\circ < \theta < 164^\circ$. The transverse-momentum resolution for full-length tracks is $\sigma(p_T)/p_T = 0.0058p_T \oplus 0.0065 \oplus 0.0014/p_T$, with p_T in GeV. The high-resolution uranium–scintillator calorimeter (CAL) [28] consists of three parts: the forward (FCAL), the barrel (BCAL) and the rear (RCAL) calorimeters. Each part is subdivided transversely into towers and longitudinally into one electromagnetic section (EMC) and either one (in RCAL) or two (in BCAL and FCAL) hadronic sections (HAC). The smallest subdivision of the calorimeter is called a cell. The CAL energy resolutions, as measured under test-beam conditions, are $\sigma(E)/E = 0.18/\sqrt{E}$ for electrons and $\sigma(E)/E = 0.35/\sqrt{E}$ for hadrons (E in GeV).

The position of positrons scattered with a small angle with respect to the positron beam direction was measured using the small-angle rear tracking detector (SRTD) [29], which also provides a means of correcting for any energy loss of the scattered positron due to the presence of inactive material. Complementing the SRTD is the rear presampler (RPRES) [30], which provides energy-loss information in RCAL regions outside the acceptance of the SRTD.

The luminosity was determined from the rate of the bremsstrahlung process $ep \rightarrow e\gamma p$, where the photon was measured with a lead-scintillator calorimeter [31] located at $Z = -107$ m.

3 Kinematics of diffractive DIS

The kinematics of the inclusive deep inelastic scattering of positrons and protons are specified by the positron-proton centre-of-mass energy, \sqrt{s} , and any two of the following variables: Q^2 , the negative square of the four-momentum of the exchanged photon; y , the inelasticity; x , the Bjorken scaling variable and W , the centre-of-mass energy of the photon-proton system.

¹ The ZEUS coordinate system is a right-handed Cartesian system, with the Z axis pointing in the proton beam direction, referred to as the “forward direction”, and the X axis pointing left towards the centre of HERA. The coordinate origin is at the nominal interaction point. The pseudorapidity is defined as $\eta = -\ln(\tan \frac{\theta}{2})$, where the polar angle, θ , is measured with respect to the proton beam direction.

Additional variables are required to describe the diffractive process $ep \rightarrow eXp$, where $X \rightarrow D^{*\pm}X'$. These are:

- t , the square of the four-momentum transfer at the proton vertex. Since t was not measured for the present data, all results discussed here are integrated over this variable;
- $x_P = (M_X^2 + Q^2)/(W^2 + Q^2)$, where M_X is the invariant mass of the hadronic final state, X , into which the virtual photon dissociates. This variable is the fraction of the proton's momentum carried by the exchanged colour-singlet system;
- $\beta = Q^2/(M_X^2 + Q^2)$ can be interpreted within the resolved-Pomeron model as the fraction of the Pomeron's momentum carried by the struck parton.

The above formulae for x_P and β neglect the proton mass and assume $t = 0$. The variables are related by $x = x_P\beta$.

To reconstruct the kinematic variables, both the final-state positron and the hadronic final state must be measured. The positron was identified using an algorithm based on a neural network [32]. The hadronic final state was reconstructed using combinations of calorimeter cells and CTD tracks to form energy-flow objects (EFOs) [4, 33]. The DIS variables were reconstructed using the double angle (DA) method [34].

The mass of the diffractive system X was calculated from the EFOs as

$$M_X^2 = \left(\sum_i E_i \right)^2 - \left(\sum_i P_{x_i} \right)^2 - \left(\sum_i P_{y_i} \right)^2 - \left(\sum_i P_{z_i} \right)^2,$$

where the sum runs over all the EFOs in the event, excluding those associated with the scattered positron.

4 Event Selection

4.1 DIS selection and $D^{*\pm}(2010)$ reconstruction

The initial event sample was selected by identifying DIS events. The selection, both online and offline, was performed in the same manner as in the inclusive DIS $D^{*\pm}$ study [15]. The only difference is in the kinematic region used, which for the present analysis is $4 < Q^2 < 400 \text{ GeV}^2$ and $0.02 < y < 0.7$.

The $D^{*\pm}$ selection cuts applied to reduce the combinatorial background differ somewhat from those used in the inclusive measurement, although the analysis is based on the same decay channel: $D^{*+} \rightarrow (D^0 \rightarrow K^- \pi^+) \pi_s^+$ (+ charge conjugate), where π_s indicates the ‘‘slow’’ pion [35]. Reduction of the combinatorial background was achieved by requiring:

- the transverse momenta of any two oppositely charged tracks, assumed to be the K and the π from the D^0 decay, to be each greater than 0.5 GeV, and the transverse momentum of the slow pion from the $D^{*\pm}$ decay to be greater than 0.12 GeV;
- $p(K\pi)/p(\pi_s) > 8$, where $p(K\pi)$ is the momentum of the candidate D^0 and $p(\pi_s)$ that of the slow pion.

Since no particle identification was performed, the K and π masses were alternately attributed to the decay products of the candidate D^0 meson. Only D^0 candidates that had an invariant mass between 1.80 GeV and 1.92 GeV were subject to the mass difference requirement $0.143 < \Delta M < 0.148$ GeV ($\Delta M = M(K\pi\pi_s) - M(K\pi)$). Further requirements placed on the $D^{*\pm}$ candidate were $1.5 < p_T(D^{*\pm}) < 8.0$ GeV and $|\eta(D^{*\pm})| < 1.5$.

After applying these requirements, a signal of 1720 ± 63 $D^{*\pm}$ mesons was obtained, using the fit procedure described in Section 4.3.

4.2 Diffractive selection

A key characteristic of a diffractive event is the presence of a large rapidity gap between the scattered proton, which remains in the forward beampipe, and the hadronic system X from the dissociated virtual photon. Such events were selected using a cut on η_{\max} , the pseudorapidity of the most-forward EFO with energy greater than 400 MeV in the event [36]. Figure 1(a) shows the distribution of η_{\max} for events containing a $D^{*\pm}$ candidate. The non-diffractive events deposit energy around the FCAL beamhole, the edge of which is located at a pseudorapidity of about four units, producing the peak at $\eta_{\max} \sim 3.5$. Below that value, the contribution from non-diffractive interactions falls exponentially [4], leaving a plateau at lower η_{\max} values, which is the signature of diffractive interactions. The shaded area in Fig. 1(a), obtained from the non-diffractive Monte Carlo simulation described in Section 5, exhibits an exponential fall-off at low η_{\max} and has no events with $\eta_{\max} < 2$, confirming that the plateau observed in the data corresponds to diffractive events. A cut of $\eta_{\max} < 2$, i.e. a gap of at least two units of pseudorapidity, was used to select diffractive events.

There are two main implications of the use of the η_{\max} selection. First, this method defines the rapidity gap with respect to the forward edge of the calorimeter and therefore cannot distinguish diffractive events in which the proton remains intact from those in which the proton dissociates into a low-mass system, whose decay products remain in the forward beampipe. To correct for this, a proton-dissociative contribution of $(31 \pm 15)\%$ [4] has been subtracted from all measured cross sections. Secondly, the η_{\max} method restricts the range of x_P values; to account for this, a cut of $x_P < 0.016$ was applied.

The presence of charm in the diffractive events automatically sets a lower limit on M_X . This, in turn, places an upper limit on the value of β of $\beta_{max} \simeq 0.96$. Since, in addition, the acceptance falls steeply at high β , only events that satisfy $\beta < 0.8$ were retained for further analysis.

4.3 $D^{*\pm}$ Signal

The ΔM distribution after all selection cuts is shown in Fig. 1(b). A clear $D^{*\pm}$ signal is evident over a small background.

To determine the number of $D^{*\pm}$ candidates, the ΔM distribution was fitted using a Gaussian function for the signal and the form

$$a(\Delta M - m_\pi)^b e^{c(\Delta M - m_\pi)}$$

for the background, where a , b and c , as well as the mean, width and normalisation of the Gaussian function were free parameters of the fit. The number of $D^{*\pm}$ candidates resulting from an unbinned log-likelihood fit was 84 ± 13 . The mean value of ΔM for the peak was 145.67 ± 0.14 MeV, consistent with the Particle Data Group (PDG) value [37]. The width of the Gaussian was 0.93 ± 0.16 MeV, in agreement with the detector resolution. The fit is good, as seen in Fig. 1(b). The same fit procedure was then followed in each cross section bin to obtain the number of $D^{*\pm}$ candidates and gave satisfactory results in each case [38]. The systematic uncertainties relating to the extraction of the number of candidates are discussed in Sect. 6.

The $K\pi$ invariant-mass distribution was fitted with a Gaussian function for the signal and a simple polynomial to describe the background. The fit to the $M(K\pi)$ distribution yielded a D^0 mass of 1865.7 ± 2.1 MeV and a resolution of 15 ± 2 MeV. The former is in good agreement with the PDG value [37], while the latter is in agreement with the detector resolution. The fit results for both the ΔM and the $M(K\pi)$ invariant-mass distributions are comparable to those found in the inclusive dataset [15, 38].

5 Monte Carlo simulation and reweighting

A GEANT-based [39] Monte Carlo (MC) simulation was used to calculate selection efficiencies and correction factors. Two different diffractive event generators were used: RIDI v2.0 [40] for evaluating the nominal correction factors and RAPGAP v2.08/01 [41] as a systematic check. For all the MC samples, events with at least one $D^{*\pm}$ decaying in the appropriate decay channel were selected and passed through the standard ZEUS detector and trigger simulations as well as the event reconstruction package.

The RIDI generator is based on the two-gluon-exchange model developed by Ryskin [40]. All stages of the parton fragmentation and hadronisation were simulated with the Lund string model [42], as implemented in JETSET [43]. The simulation included QED radiative corrections. Separate samples of $\gamma^* \rightarrow q\bar{q}$ and $\gamma^* \rightarrow q\bar{q}g$ interactions were generated. The CTEQ4LQ [44] proton parton distribution functions were used as input and the charm mass (m_c) was set to 1.35 GeV. The acceptance corrections have little sensitivity to the value chosen for m_c .

The distributions of the variables Q^2 , x_P and β from the $q\bar{q}$ and $q\bar{q}g$ RIDI MC samples are compared to the data in Fig. 2. Neither MC sample alone reproduces the measurements, particularly the β distribution. Therefore, the two RIDI MC samples were combined by fitting the fraction of $q\bar{q}$ events in the three bins of Q^2 used to extract the differential cross sections. The x_P distribution in each Q^2 bin was used in making the fit. It was found that neither reweighting in β nor in x_P separately gave a good description of the detector-level distributions in the data. The fraction of $q\bar{q}$ events increases with Q^2 from approximately 4% in the lowest- Q^2 bin to around 50% in the highest- Q^2 bin. This mixed sample, shown as the hatched histograms in Fig. 2, is in satisfactory agreement with the data. The acceptance in the kinematic region used for the cross-section measurement was 17.3%.

The RAPGAP simulation provides a rather general framework for the generation of diffractive events. The resolved-Pomeron option was used, in which charm quarks are produced via the leading-order BGF process. Charm fragmentation was carried out using the Peterson fragmentation model with the parameter ϵ_c set to 0.035 [45]. The fragmentation process was simulated using the colour-dipole model implemented in ARIADNE [46] and the hadronisation was carried out according to the Lund string model. The sample was generated assuming a gluon-dominated Pomeron, with a gluon distribution peaked close to $\beta = 1$ [5, 6]. The Pomeron intercept was set to $\alpha_P(0) = 1.20$ and the charm mass was set to 1.35 GeV. The QED radiative corrections are not available for diffractive charm production in RAPGAP.

Similar discrepancies to those observed in the original RIDI samples were seen when comparing the RAPGAP MC sample to the data, with the exception that the x_P distribution was well described. To correct for the discrepancies, the RAPGAP sample was simultaneously reweighted in $\log Q^2$ and M_X , after which agreement was obtained in all distributions.

The RAPGAP generator, which also simulates non-diffractive interactions, was used to produce a non-diffractive $D^{*\pm}$ sample for the extraction of the ratio of diffractive to inclusive $D^{*\pm}$ production (see Section 7.2). The parameters used were the same as those used in the measurement of the inclusive DIS $D^{*\pm}$ cross sections [15].

6 Systematic uncertainties on the cross section measurements

The major sources of systematic uncertainties and their effect on the measurement of the cross section are:

- the selection of inclusive DIS events. These systematic uncertainties were derived in the same way as for the inclusive DIS $D^{*\pm}$ analysis [15] and resulted in an overall variation in the cross section of $^{+2\%}_{-9\%}$;
- the selection of $D^{*\pm}$ candidates. The minimum transverse momentum of tracks used in the $D^{*\pm}$ reconstruction was raised and lowered by 15% and the threshold on the momentum-ratio $p(K\pi)/p(\pi_s)$ was increased by 0.5 units². These variations yielded a combined uncertainty of $\pm 6\%$;
- the selection of diffractive events. The η_{\max} requirement was varied by ± 0.2 units and the EFO energy threshold applied in the reconstruction of η_{\max} was varied by ± 100 MeV. The combined effect of these changes was $^{+8\%}_{-6\%}$;
- the model dependence of the corrections. This uncertainty was estimated using the reweighted diffractive RAPGAP sample instead of the mixed RIDI sample. This change resulted in a variation of -9% ;
- the reweighting procedure. The $q\bar{q}$ fraction in each Q^2 bin was separately varied up and down by its uncertainty as determined from the fit (see Section 5). The resulting deviations were summed in quadrature, giving a variation of $^{+5\%}_{-4\%}$.

These systematic uncertainties were added in quadrature separately for the positive and negative deviations from the nominal values of the cross section to determine the overall systematic uncertainty of $^{+11\%}_{-16\%}$. These estimates were also done in each bin in which the cross section was measured. The sources of systematic uncertainty relating to the extraction of the number of $D^{*\pm}$ candidates were also considered, but were found to be negligible in comparison to those listed above.

The overall normalisation uncertainties arising from the uncertainties on the luminosity measurement and the $D^{*\pm}$ and D^0 branching fractions were not included in the systematic uncertainty. The uncertainty arising from the subtraction of proton-dissociative background, quoted separately, is $\pm 22\%$ [4].

7 Results

² A trigger requirement did not permit the decrease of this momentum-ratio cut.

7.1 Cross sections

The differential cross sections in any given variable ξ were determined using

$$\frac{d\sigma}{d\xi} = \frac{N_D(1 - f_{\text{pdiss}})}{A \cdot \mathcal{L} \cdot B \cdot \delta\xi}, \quad (1)$$

where N_D is the number of $D^{*\pm}$ candidates fit in a bin of width $\delta\xi$, A is the correction factor (accounting for acceptance, migrations, efficiencies and radiative effects) for that bin, \mathcal{L} is the integrated luminosity and $B = 2.59 \pm 0.06\%$ is the total $D^{*+} \rightarrow D^0\pi_s^+ \rightarrow (K^-\pi^+)\pi_s^+$ branching ratio [37]. The quantity f_{pdiss} is the fraction of proton-dissociative background. All other sources of background were neglected.

Figure 3 shows the measured differential $D^{*\pm}$ cross sections with respect to the kinematic variables Q^2 , W , $x_{\mathcal{P}}$, β , $p_T(D^{*\pm})$ and $\eta(D^{*\pm})$. The values are also given in Table 1. The data exhibit a sharp fall-off as a function of Q^2 and $p_T(D^{*\pm})$. The events are concentrated at low β , but are uniformly distributed in $x_{\mathcal{P}}$, within the large uncertainties. The W dependence is mainly determined by the $p_T(D^{*\pm})$ and $\eta(D^{*\pm})$ restrictions.

The cross section for diffractive $D^{*\pm}$ production in the kinematic region $4 < Q^2 < 400 \text{ GeV}^2$, $0.02 < y < 0.7$, $1.5 < p_T(D^{*\pm}) < 8 \text{ GeV}$, $|\eta(D^{*\pm})| < 1.5$, $x_{\mathcal{P}} < 0.016$ and $\beta < 0.8$ is

$$\sigma_{ep \rightarrow eD^{*\pm}X'p} = 291 \pm 44(\text{stat.})_{-47}^{+32}(\text{syst.}) \pm 63(\text{prot. diss.}) \text{ pb}, \quad (2)$$

where the last uncertainty arises from the subtraction of the background from proton dissociation.

7.2 Ratio of diffractive to inclusive $D^{*\pm}$ production.

The ratio of diffractive to inclusive $D^{*\pm}$ production was measured for $x < 0.0128$. This limit is equivalent to the $x_{\mathcal{P}}$ and β requirements imposed on the diffractive sample. In the kinematic region $4 < Q^2 < 400 \text{ GeV}^2$, $0.02 < y < 0.7$, $1.5 < p_T(D^{*\pm}) < 8 \text{ GeV}$, $|\eta(D^{*\pm})| < 1.5$ and $x < 0.0128$, the inclusive DIS $D^{*\pm}$ cross section is $\sigma_{ep \rightarrow eD^{*\pm}Y} = 4.83 \pm 0.18(\text{stat.}) \text{ nb}$, where Y is the complete hadronic final state except for the tagged $D^{*\pm}$ meson. This value is consistent with an earlier ZEUS measurement [15], taking into account the differences between the two kinematic regions. The ratio of diffractive to inclusive DIS $D^{*\pm}$ production is then defined by

$$R_D = \frac{\sigma_{ep \rightarrow eD^{*\pm}X'p}(x_{\mathcal{P}} < 0.016, \beta < 0.8)}{\sigma_{ep \rightarrow eD^{*\pm}Y}(x < 0.0128)}. \quad (3)$$

It is assumed that all the systematic uncertainties, except those relating to the diffractive selection and the MC reweighting, cancel. This is a reasonable approximation given that

the cross section results in the diffractive case are statistically limited. The measured ratio is therefore

$$R_D = 6.0 \pm 0.9(\text{stat.})_{-0.7}^{+0.5}(\text{syst.}) \pm 1.3(\text{prot. diss.})\%. \quad (4)$$

Figure 4 shows R_D as a function of Q^2 and W .

8 Discussion

Three models are compared to the measured cross sections: (1) the resolved-Pomeron model, as implemented in the fits to HERA data made by Alvero et al. (ACTW) [47], (2) the two-gluon-exchange “saturation” model of Golec-Biernat and Wüsthoff [48], as implemented in the SATRAP MC generator and interfaced to RAPGAP [49] and (3) the two-gluon-exchange model of Bartels et al. (BJLW) [14, 50], as implemented in RAPGAP.

The version of SATRAP used is the same as that used in the recent ZEUS publication on the study of hadronic final states in diffraction [7], where it is referred to as “SATRAP-CDM”. Although the SATRAP and BJLW predictions are both based on two-gluon exchange, they differ in the treatment of the $q\bar{q}g$ final state, which is an important contributor to charm production. In the SATRAP-CDM model, only configurations in which the transverse momenta satisfy $k_T(q), k_T(\bar{q}) > k_T(g)$ are included in the calculation of the $q\bar{q}g$ final state, while all configurations with $k_T(g) > 1 \text{ GeV}$ are used in the BJLW model.

The predicted cross sections from three of the fits by Alvero et al. are shown in Table 2. The calculations were made assuming $m_c = 1.45 \text{ GeV}$ and the Peterson fragmentation model (with the parameter $\epsilon_c = 0.035$) for the charm decay. The probability for charm to fragment into a $D^{*\pm}$ meson was taken as 0.235 [51] and the renormalisation and factorisation scales were set to $\mu_R = \mu_F = \sqrt{Q^2 + 4m_c^2}$. Varying the charm mass by $\pm 0.15 \text{ GeV}$ gave a ${}_{-17}^{+18}\%$ variation in each cross section. The theoretical uncertainties relating to the scale and the value of the Pomeron intercept are comparable to that arising from the charm mass. Fits B and D, which assume a gluon-dominated Pomeron, are favoured by the data. The fit SG, which assumes a Pomeron dominated by gluons with a “superhard” density, predicts too small a cross section. A quark-dominated Pomeron (not shown) predicts a cross section too small by two orders of magnitude.

Table 2 also shows the predicted cross sections from SATRAP-CDM and the BJLW model, along with the $q\bar{q}$ contribution from the BJLW calculations. The same assumptions are made in these calculations as were made in the ACTW case, except that here $\mu_R = \mu_F = Q$. The BJLW $q\bar{q}$ contribution is clearly too small, while the sum of the $q\bar{q}$ and $q\bar{q}g$ BJLW

contributions gives good agreement with the data. The SATRAP-CDM and ACTW fit B predictions are smaller than the data, but not significantly so.

Figure 3 compares the predictions of ACTW fit B, SATRAP-CDM and BJLW, along with the $q\bar{q}$ BJLW contribution, with the measured differential $D^{*\pm}$ cross sections. The ACTW fit B and fit D predict similar shapes for the differential distributions and therefore no comparisons with fit D are made. The ACTW and SATRAP-CDM predictions are in reasonable agreement with the measured differential distributions, with the exception of the β distribution, where both predictions undershoot the data at high β . The $q\bar{q}$ contribution from the BJLW calculations clearly fails to describe the shape of the distributions, particularly that for β . The sum of the two BJLW contributions gives a good representation of all the measured distributions.

The ratio, R_D , agrees with that determined in inclusive diffraction [4], indicating that charm production is not suppressed in diffractive DIS, contrary to the expectations of some early models [22]. Figure 4 shows that R_D is consistent with being independent of Q^2 and W .

The H1 Collaboration recently published similar results [25]. The kinematic region in that study is significantly different to that used here, making it difficult to compare the results directly. However, comparisons with Monte Carlo models indicate that the two sets of results are consistent.

9 Summary

The cross section for diffractive $D^{*\pm}$ production in the kinematic region, $4 < Q^2 < 400 \text{ GeV}^2$, $0.02 < y < 0.7$, $x_P < 0.016$, $\beta < 0.8$, $1.5 < p_T(D^{*\pm}) < 8 \text{ GeV}$ and $|\eta(D^{*\pm})| < 1.5$ has been measured to be $291 \pm 44(\text{stat.})_{-47}^{+32}(\text{syst.}) \pm 63(\text{prot. diss.}) \text{ pb}$. Differential cross sections have been compared to the predictions of different models of diffractive charm production. The resolved-Pomeron model of Alvero et al. is below the data at high β . In the case of the two-gluon-exchange models, the $q\bar{q}$ contribution alone gives too small a cross section. Inclusion of the $q\bar{q}g$ contribution results in a good description of the data by the BJLW prediction, while the SATRAP-CDM prediction undershoots the data, particularly at high β .

The ratio of diffractive $D^{*\pm}$ production to inclusive DIS $D^{*\pm}$ production is $R_D = 6.0 \pm 0.9(\text{stat.})_{-0.7}^{+0.5}(\text{syst.}) \pm 1.3(\text{prot. diss.}) \%$. This result is in agreement with the corresponding ratio for inclusive diffraction, indicating that charm production in diffraction is not suppressed with respect to light-flavour production. The ratio R_D is independent of Q^2 and W within the uncertainties.

Acknowledgments

We thank the DESY Directorate for their strong support and encouragement, and the HERA machine group for their diligent efforts. We are grateful for the support of the DESY computing and network services. The design, construction and installation of the ZEUS detector have been made possible owing to the ingenuity and effort of many people from DESY and home institutes who are not listed as authors. It is also a pleasure to thank L. Alvero, J. Bartels, J. Collins, A. Hebecker, H. Jung, M. McDermott and M. Ryskin for useful discussions.

References

- [1] ZEUS Coll., M. Derrick et al., *Z. Phys.* **C 68**, 569 (1995).
- [2] H1 Coll., T. Ahmed et al., *Phys. Lett.* **B 348**, 681 (1995).
- [3] ZEUS Coll., M. Derrick et al., *Z. Phys.* **C 70**, 391 (1996).
- [4] ZEUS Coll., J. Breitweg et al., *Eur. Phys. J.* **C 6**, 43 (1999).
- [5] H1 Coll., C. Adloff et al., *Phys. Lett.* **B 428**, 206 (1998).
- [6] H1 Coll., C. Adloff et al., *Z. Phys.* **C 76**, 613 (1997).
- [7] ZEUS Coll., S. Chekanov et al., *Phys. Rev.* **D 65**, 052001 (2002).
- [8] A. Donnachie and P.V. Landshoff, *Nucl. Phys.* **B 231**, 189 (1984);
A. Donnachie and P.V. Landshoff, *Phys. Lett.* **B 296**, 227 (1992).
- [9] W. Buchmüller, A. Hebecker and M.F. McDermott, *Phys. Lett.* **B 404**, 353 (1997).
- [10] M. Diehl, *Eur. Phys. J.* **C 1**, 293 (1998).
- [11] E.M. Levin et al., *Z. Phys.* **C 74**, 671 (1997).
- [12] L.P.A. Haakman, A.B. Kaidalov and J.H. Koch, *Eur. Phys. J.* **C 1**, 547 (1998).
- [13] M. Genovese, N.N. Nikolaev and B.G. Zakharov, *Phys. Lett.* **B 378**, 347 (1996).
- [14] H. Lotter, *Phys. Lett.* **B 406**, 171 (1997);
J. Bartels, H. Jung and M. Wüsthoff, *Eur. Phys. J.* **C 11**, 111 (1999);
J. Bartels, H. Jung and A. Kyrieleis, Preprint DESY-01-116 (hep-ph/0010300), 2000.
- [15] ZEUS Coll., J. Breitweg et al., *Eur. Phys. J.* **C 12**, 35 (2000).
- [16] H1 Coll., C. Adloff et al., *Nucl. Phys.* **B 545**, 21 (1999).
- [17] G. Ingelman and P.E. Schlein, *Phys. Lett.* **B 152**, 256 (1985).
- [18] V.N. Gribov and L.N. Lipatov, *Sov. J. Nucl. Phys.* **15**, 438 (1972);
L.N. Lipatov, *Sov. J. Nucl. Phys.* **20**, 94 (1975);
Yu.L. Dokshitzer, *Sov. Phys. JETP* **46**, 641 (1977);
G. Altarelli and G. Parisi, *Nucl. Phys.* **B 126**, 298 (1977).
- [19] ZEUS Coll., M. Derrick et al., *Phys. Lett.* **B 356**, 129 (1995).
- [20] See e.g., *Proc. HERA Workshop*, G. Ingelman, A. De Roeck and R. Klanner (eds.), Vol. 2, p. 635. DESY (1996). See also references therein.
- [21] F.E. Low, *Phys. Rev.* **D 12**, 163 (1975);
S. Nussinov, *Phys. Rev. Lett.* **34**, 1286 (1975);
S. Nussinov, *Phys. Rev.* **D 14**, 246 (1976).

- [22] N.N. Nikolaev and B.G. Zakharov, *Z. Phys.* **C 53**, 331 (1992).
- [23] M. Genovese, N.N. Nikolaev and B.G. Zakharov, *Sov. Phys. JETP* **81**, 625 (1995).
- [24] A. Edin, G. Ingelman and J. Rathsmann, *Phys. Lett.* **B 366**, 371 (1996).
- [25] H1 Coll., C. Adloff et al., *Phys. Lett.* **B 520**, 191 (2001).
- [26] ZEUS Coll., U. Holm (ed.), *The ZEUS Detector*. Status Report (unpublished), DESY (1993), available on <http://www-zeus.desy.de/bluebook/bluebook.html>.
- [27] N. Harnew et al., *Nucl. Inst. Meth.* **A 279**, 290 (1989);
B. Foster et al., *Nucl. Phys. Proc. Suppl.* **B 32**, 181 (1993);
B. Foster et al., *Nucl. Inst. Meth.* **A 338**, 254 (1994).
- [28] M. Derrick et al., *Nucl. Inst. Meth.* **A 309**, 77 (1991);
A. Andresen et al., *Nucl. Inst. Meth.* **A 309**, 101 (1991);
A. Caldwell et al., *Nucl. Inst. Meth.* **A 321**, 356 (1992);
A. Bernstein et al., *Nucl. Inst. Meth.* **A 336**, 23 (1993).
- [29] A. Bamberger et al., *Nucl. Inst. Meth.* **A 401**, 63 (1997).
- [30] A. Bamberger et al., *Nucl. Inst. Meth.* **A 382**, 419 (1996).
- [31] J. Andruszków et al., Preprint DESY-92-066, DESY, 1992;
ZEUS Coll., M. Derrick et al., *Z. Phys.* **C 63**, 391 (1994);
J. Andruszków et al., *Acta Phys. Pol.* **B 32**, 2025 (2001).
- [32] H. Abramowicz, A. Caldwell and R. Sinkus, *Nucl. Inst. Meth.* **A 365**, 508 (1995).
- [33] G.M. Briskin, *Diffractional Dissociation in ep Deep Inelastic Scattering*. Ph.D. Thesis, Tel Aviv University, 1998. (Unpublished);
ZEUS Coll., J. Breitweg et al., *Eur. Phys. J.* **C 1**, 81 (1998).
- [34] S. Bentvelsen, J. Engelen and P. Kooijman, *Proc. Workshop on Physics at HERA*, W. Buchmüller and G. Ingelman (eds.), Vol. 1, p. 23. Hamburg, Germany, DESY (1992);
K.C. Höger, *Proc. Workshop on Physics at HERA*, W. Buchmüller and G. Ingelman (eds.), Vol. 1, p. 43. Hamburg, Germany, DESY (1992).
- [35] S. Nussinov, *Phys. Rev. Lett.* **35**, 1672 (1975).
- [36] ZEUS Coll., M. Derrick et al., *Phys. Lett.* **B 315**, 481 (1993);
ZEUS Coll., M. Derrick et al., *Phys. Lett.* **B 332**, 228 (1994).
- [37] Particle Data Group, D.E. Groom et al., *Eur. Phys. J.* **C 15**, 1 (2000).
- [38] J.E. Cole, *Open Charm Production in Deep Inelastic Diffractive ep Scattering at HERA*. Thesis, University of London, Report RAL-TH-1999-008, 1999.
- [39] R. Brun et al., GEANT3, Technical Report CERN-DD/EE/84-1, CERN, 1987.

- [40] M.G. Ryskin, *Sov. J. Nucl. Phys.* **52**, 529 (1990);
M.G. Ryskin, S.Y. Sivoklokov and A. Solano, *Proc. International Conf. on Elastic and Diffractive Scattering, Providence RI, June 1993*, H.M. Fried, K. Kang and C.I. Tan (eds.). World Scientific, Singapore (1993);
M.G. Ryskin and A. Solano, *Proc. Workshop on Monte Carlo Generators for HERA Physics*, G. Grindhammer, G. Ingelman, H. Jung and T. Doyle (eds.), p. 386. DESY, Hamburg, Germany (1999). Also in preprint DESY-PROC-1999-02, available on <http://www.desy.de/~heramc/>.
- [41] H. Jung, *Comp. Phys. Comm.* **86**, 147 (1995).
- [42] B. Andersson et al., *Phys. Rep.* **97**, 31 (1983).
- [43] T. Sjöstrand, *Comp. Phys. Comm.* **82**, 74 (1994).
- [44] H.L. Lai et al., *Phys. Rev.* **D 55**, 1280 (1997).
- [45] C. Peterson et al., *Phys. Rev.* **D 27**, 105 (1983);
OPAL Coll., R. Akers et al., *Z. Phys.* **C 67**, 27 (1995).
- [46] L. Lönnblad, *Comp. Phys. Comm.* **71**, 15 (1992).
- [47] L. Alvero et al., *Phys. Rev.* **D 59**, 074022 (1999);
L. Alvero, J.C. Collins and J.J. Whitmore, Preprint hep-ph/9806340, 1998.
- [48] K. Golec-Biernat and M. Wüsthoff, *Phys. Rev.* **D 59**, 014017 (1999);
K. Golec-Biernat and M. Wüsthoff, *Phys. Rev.* **D 60**, 114023 (1999).
- [49] H. Kowalski, *Proceedings of the Workshop on New Trends in HERA Physics*, G. Grindhammer, B.A. Kniehl and G. Kramer (eds.), pp. 361–380. (1999), available on <http://www-library.desy.de/conf/ringberg99.html>;
H. Kowalski and M. Wüsthoff, *Proceedings of the 8th International Workshop Deep Inelastic Scattering and QCD*, J. Gracey and T. Greenshaw (eds.), p. 192. World Scientific, Singapore (2000).
- [50] J. Bartels, H. Lotter and M. Wüsthoff, *Phys. Lett.* **B 379**, 239 (1996);
J. Bartels et al., *Phys. Lett.* **B 386**, 389 (1996).
- [51] L. Gladilin, Preprint hep-ex/9912064, 1999.

$d\sigma/dQ^2$		
Q^2 Range (GeV ²)	Q^2 (GeV ²)	σ (pb)
4 - 12	6.7	$131 \pm 32^{+35}_{-38} \pm 28$
12 - 25	17.8	$95 \pm 21^{+19}_{-32} \pm 21$
25 - 400	67.7	$64 \pm 18^{+10}_{-7} \pm 14$
$d\sigma/dW$		
W Range (GeV)	W (GeV)	σ (pb)
50 - 130	97.4	$121 \pm 41^{+36}_{-59} \pm 26$
130 - 170	149.3	$84 \pm 20^{+8}_{-21} \pm 18$
170 - 250	213.9	$97 \pm 27^{+16}_{-25} \pm 21$
$d\sigma/dx_{\mathcal{P}}$		
$x_{\mathcal{P}}$ Range	$x_{\mathcal{P}}$	σ (pb)
0 - 0.0045	0.0031	$99 \pm 26^{+14}_{-21} \pm 22$
0.0045 - 0.009	0.0066	$68 \pm 17^{+43}_{-18} \pm 15$
0.009 - 0.016	0.0123	$150 \pm 34^{+32}_{-109} \pm 33$
$d\sigma/d\beta$		
β Range	β	σ (pb)
0 - 0.1	0.043	$129 \pm 31^{+22}_{-47} \pm 28$
0.1 - 0.3	0.19	$72 \pm 16^{+16}_{-6} \pm 16$
0.3 - 0.8	0.50	$81 \pm 20^{+9}_{-12} \pm 18$
$d\sigma/dp_T(D^{*\pm})$		
$p_T(D^{*\pm})$ Range (GeV)	$p_T(D^{*\pm})$ (GeV)	σ (pb)
1.5 - 2.4	1.9	$149 \pm 49^{+152}_{-45} \pm 32$
2.4 - 3.6	2.8	$81 \pm 20^{+9}_{-13} \pm 18$
3.6 - 8.0	4.4	$52 \pm 11^{+5}_{-10} \pm 11$
$d\sigma/d\eta(D^{*\pm})$		
$\eta(D^{*\pm})$ Range	$\eta(D^{*\pm})$	σ (pb)
-1.5 - -0.65	-0.98	$106 \pm 28^{+9}_{-20} \pm 23$
-0.65 - 0.1	-0.24	$95 \pm 21^{+11}_{-37} \pm 21$
0.1 - 1.5	0.79	$76 \pm 23^{+31}_{-17} \pm 17$

Table 1: Values of the differential cross sections with respect to Q^2 , W , $x_{\mathcal{P}}$, β , $p_T(D^{*\pm})$ and $\eta(D^{*\pm})$. The following quantities are given: the range of the measurement; the value at which the cross section is quoted and the measured cross section. The first uncertainty quoted represents the statistical uncertainty, the second the systematic and the third the uncertainty arising from the subtraction of the proton dissociation background.

	Cross Section (pb)
Data	$291 \pm 44^{+32}_{-47} \pm 63$
ACTW FIT B	187
ACTW FIT D	401
ACTW FIT SG	87
SATRAP	185
BJLW $q\bar{q}$	79
BJLW $q\bar{q} + q\bar{q}g$	297

Table 2: *Comparison of the measured cross section with those predicted by the models described in the text. No errors are quoted given the considerable flexibility in the predicted cross sections depending upon the choice of input parameters for the models.*

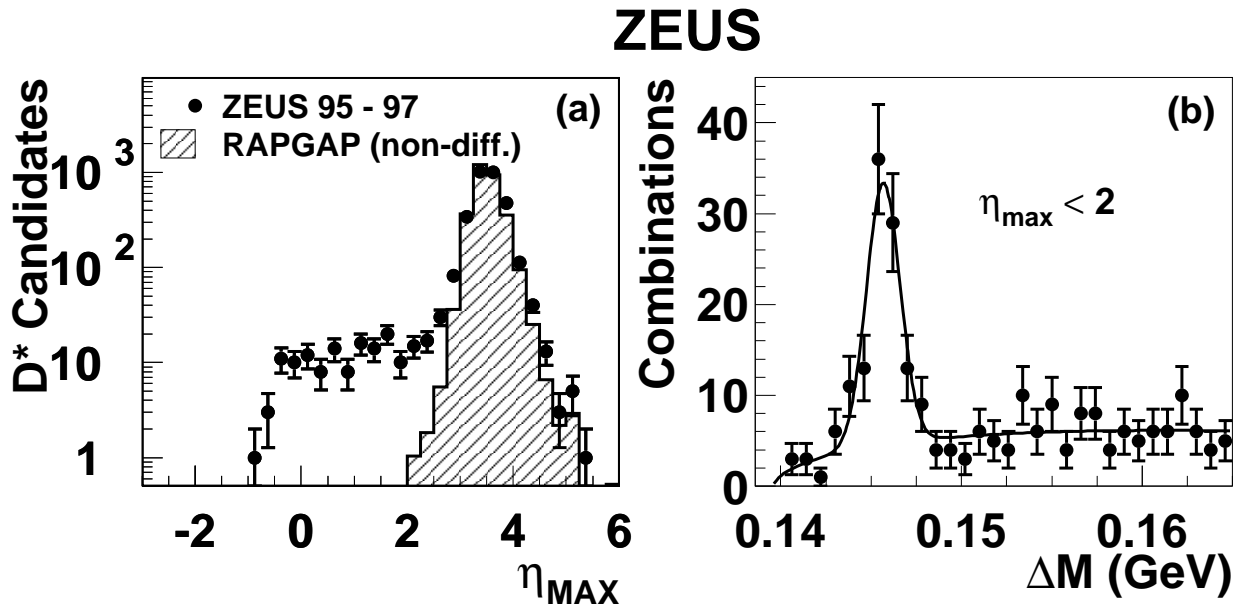


Figure 1: (a) The η_{max} distribution for DIS events with a $D^{*\pm}$ candidate. The shaded histogram is the prediction from the RAPGAP non-diffractive Monte Carlo simulation (see section 5). (b) The ΔM distribution for events with $\eta_{\text{max}} < 2$. Only the combinations whose values of $M(K\pi)$ lie in the signal region are included. The curve shows the unbinned log-likelihood fit described in the text.

ZEUS

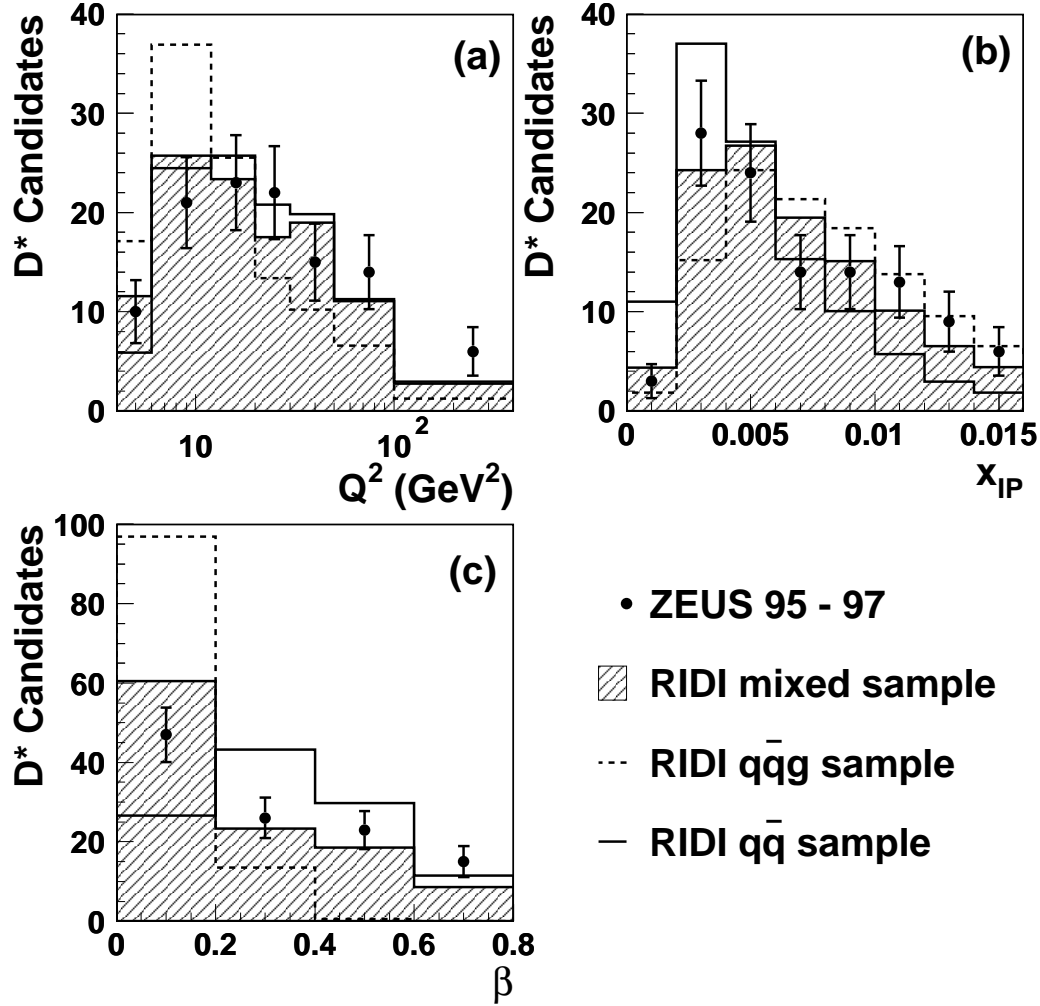


Figure 2: The Q^2 , x_{IP} and β distributions at the detector level for the data and the RIDI MC samples. The data sample is shown as the solid points and the $q\bar{q}$ and $q\bar{q}\gamma$ RIDI samples are shown separately as the solid and dashed histograms. The mixed sample, produced according to the procedure described in the text, is shown as the hatched histograms. All the MC distributions have been normalised to the number of events in the data.

ZEUS

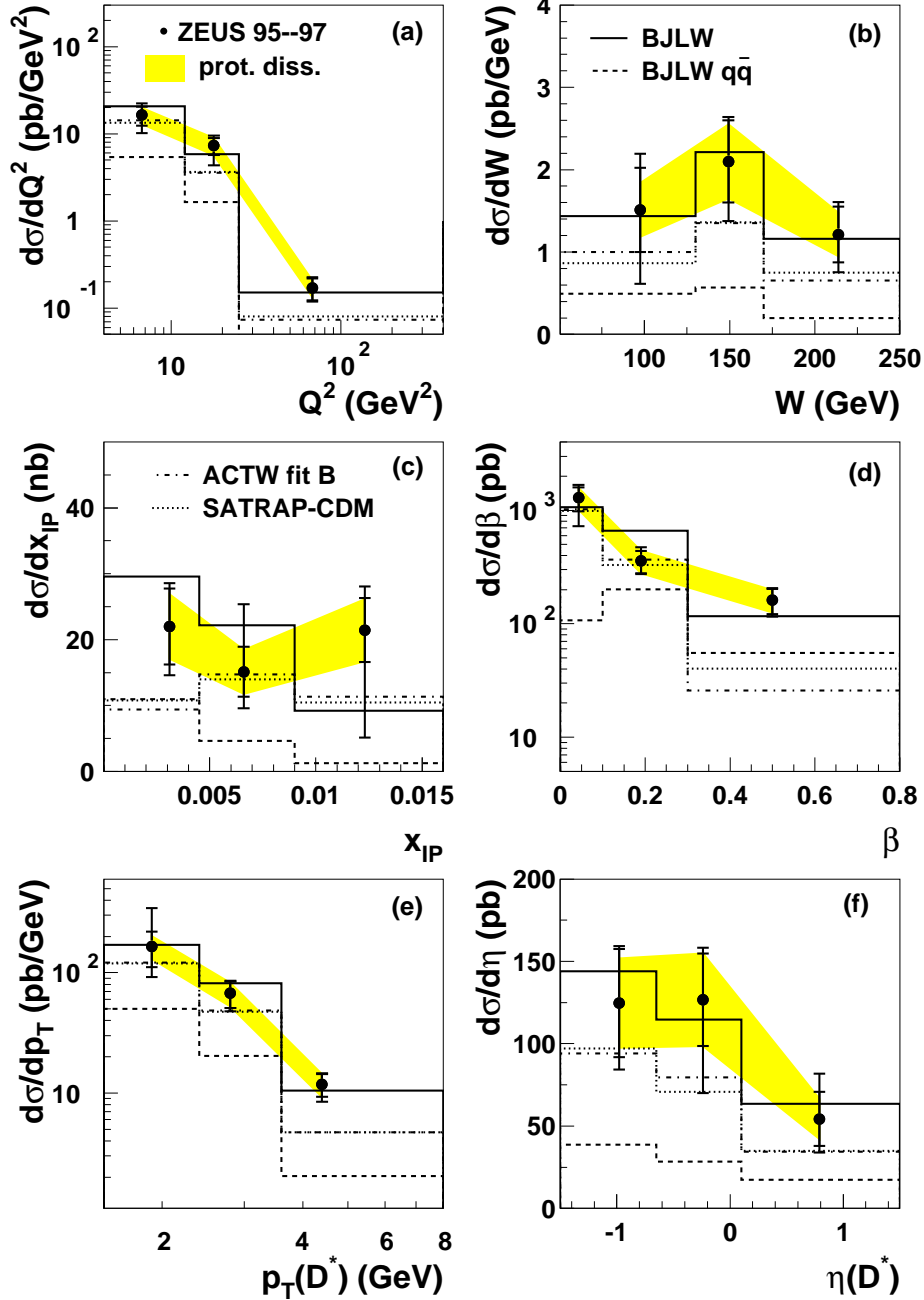


Figure 3: *Differential cross sections for $D^{*\pm}$ production in the kinematic region described in the text. The cross sections are shown as a function of (a) Q^2 , (b) W , (c) x_P , (d) β , (e) $p_T(D^{*\pm})$ and (f) $\eta(D^{*\pm})$. The inner bars show the statistical uncertainties, while the outer bars indicate the statistical and systematic uncertainties added in quadrature. The shaded bands show the uncertainty coming from the subtraction of the proton-dissociation background. The histograms correspond to the different models described in the text.*

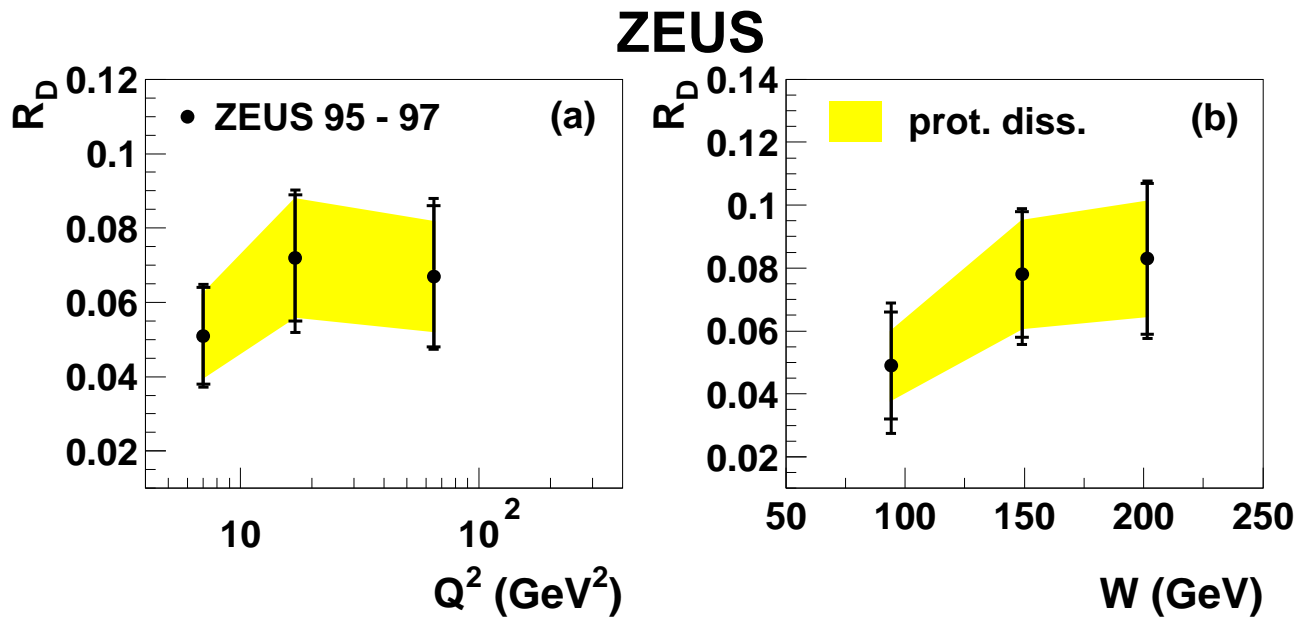


Figure 4: *The measured ratio of diffractively produced $D^{*\pm}$ mesons to inclusive $D^{*\pm}$ meson production, R_D , as a function of Q^2 and W . The inner bars indicate the statistical uncertainties, while the outer ones indicate the statistical and systematic uncertainties added in quadrature. The shaded band indicates the uncertainty arising from the subtraction of the proton-dissociation background.*